Journal of Materials Chemistry A

Accepted Manuscript

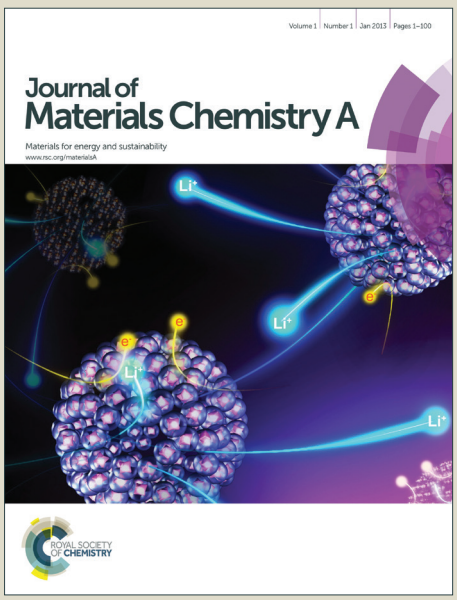

ROYAL SOCIETY OF CHEMISTRY

www.rsc.org/materialsA

Journal Name

RSCPublishing

COMMUNICATION

Electrospun Nanofibrous Adsorbent for Uranium Extraction from Seawater

Cite this: DOI: 10.1039/x0xx00000x

Siyuan XIE,‡[a,b] Xiyan LIU,‡[a] Bowu ZHANG,*[a] Hongjuan MA,[a] Changjian LING,[a] Ming YU,[a] Linfan LI[a] and Jingye LI*[a]

Received 00th January 2012,
Accepted 00th January 2012

DOI: 10.1039/x0xx00000x

www.rsc.org/

Here we firstly report a nanoadsorbent design, integrating the high affinity of amidoxime (AO) groups and size effect of nanomaterials in nanofibrous composite mats prepared by two-nozzle electrospinning process, for the adsorption test of uranium in simulated seawater with an uptake capacity of 1.6 mg U g^{-1} adsorbent in the presence of massive interference ions.

The ocean is a vast repository of uranium, containing, at an estimated 4.5 billion tons, thousands of times to the identified terrestrial reserves.[1] The extraction of uranium from seawater has been explored since the first half of last century,[2] but it is still far from an economical method of uranium production. Because the uranium concentration in real seawater is minuscule at 3.3 parts per billion, extraction processes are inefficient, resulting in high costs.[3, 4] Over the past few decades, AO-based adsorbents have been proved as the most promising candidates for uranium extraction, because of its high uptake of uranyl ions, rapid adsorption rate, high selectivity, easy handling, and safety of the environment.[5] Adsorption by AO-based adsorbents has been considered as the most promising method to recover uranium from seawater.[6, 7, 8] Japanese scientists designed a fabric/fiber absorbent to accomplish this uranium extraction, in which acrylonitrile (AN) was graft-polymerized onto polyethylene fabric or fiber using electron beam or gamma ray irradiation and then converted into AO groups by chemical processes.[8, 9, 10] These fabric or fiber absorbents possess both the absorption properties of AO groups and mechanical strength of polyethylene, which imparted durability in actual conditions. Marine tests showed that the uranium uptake by these fiber adsorbents assembled as a braided system was 1.5 g U kg^{-1} adsorbent after 30 days soaking at 30°C in the Okinawa area.[4] Likewise, American and Chinese scientists also have engaged in the development of AO-based adsorbents by a similar method.[11, 12] In contrast to the uranium enrichment in terrestrial ores, more work is necessary to improve the adsorption performance of AO-based adsorbents in actual seawater in order to make uranium recovery more economical.[13]

Uranium adsorption from seawater is controlled by dynamics; therefore, the design of adsorbents with large surface areas appears to be a plausible route to improve adsorption efficiency. To date, many nanomaterials have been used and proven to be very effective for uranium recovery, including multi-walled carbon nanotubes,[14, 15] graphene oxide,[16] metal organic frameworks, [17] and other in-/organic nanospheres.[18, 19] S. Dai *et al.* designed a novel mesoporous adsorbent beginning with a porous polymer framework as initiator to graft-polymerize AN by atom-transfer radical polymerization (ATRP), followed by conversion to an AO-based mesoporous adsorbent. The obtained adsorbent possessed a higher surface area and pore volume in comparison with nonporous material. Tests with simulated seawater evidenced its distinctly higher and significantly faster uranium adsorption compared to conventional, polyethylene-based adsorbents.[20] Similarly, they prepared another mesoporous AO-based adsorbent by immobilizing acrylonitrile and acrylic acid copolymers, which divinylbenzene was used as cross-linker, onto a mesoporous carbon framework. Uranium adsorption results shown that the adsorption capacities are strongly influenced by the density of the AO groups and the specific surface area.[21] The good adsorption capacities of these nanomaterials have been shown in laboratory studies, and indicate the potential of these novel AO-based adsorbents.[14, 16, 19, 20, 21] Therefore, the design of adsorbents with not only the high adsorption properties of nanomaterials but also the packing and durability advantages of the bulk materials would be a key strategy for preparing practical and efficient uranium extraction materials.

Electrospinning is a process in which viscous polymer fluid overcomes surface tension through electrostatic traction to produce a continuous jet that is drawn out into ultrafine fibers.[22] These ultrafine fibers can be assembled randomly or directionally into a large-scale mat (from several centimeters to meters in size).[23, 24] The nanofibrous mat is generally considered to be a highly porous material (~80% porosity),[25, 26] and the pores are essentially interfibers spaces with dimensions that commonly range from several hundred nanometers to a few micrometers. Thus, electrospinning is a powerful approach for preparing nanomaterials on large-scale, while still retaining the

effects of an extremely large surface ratio in macroscopic assembly.[23, 27] Remarkably, some functional materials prepared though electrospinning have been used as adsorbent and catalyst support.[28]

Using commercial polyacrylonitrile (PAN) as a starting material perfectly dovetails with the electrospinning technology for the preparation of AO-based adsorbents. After the amidoximation of PAN, we found the resultant product, polyamidoxime (PAO), to be very stiff and breakable. This material cannot be used directly as an adsorbent unless a skeletal component is introduced to reinforce its mechanical strength. Unfortunately, the conventional blending solution is impracticable here, because we further determined that PAO was quite immiscible with many other polymers in solution.

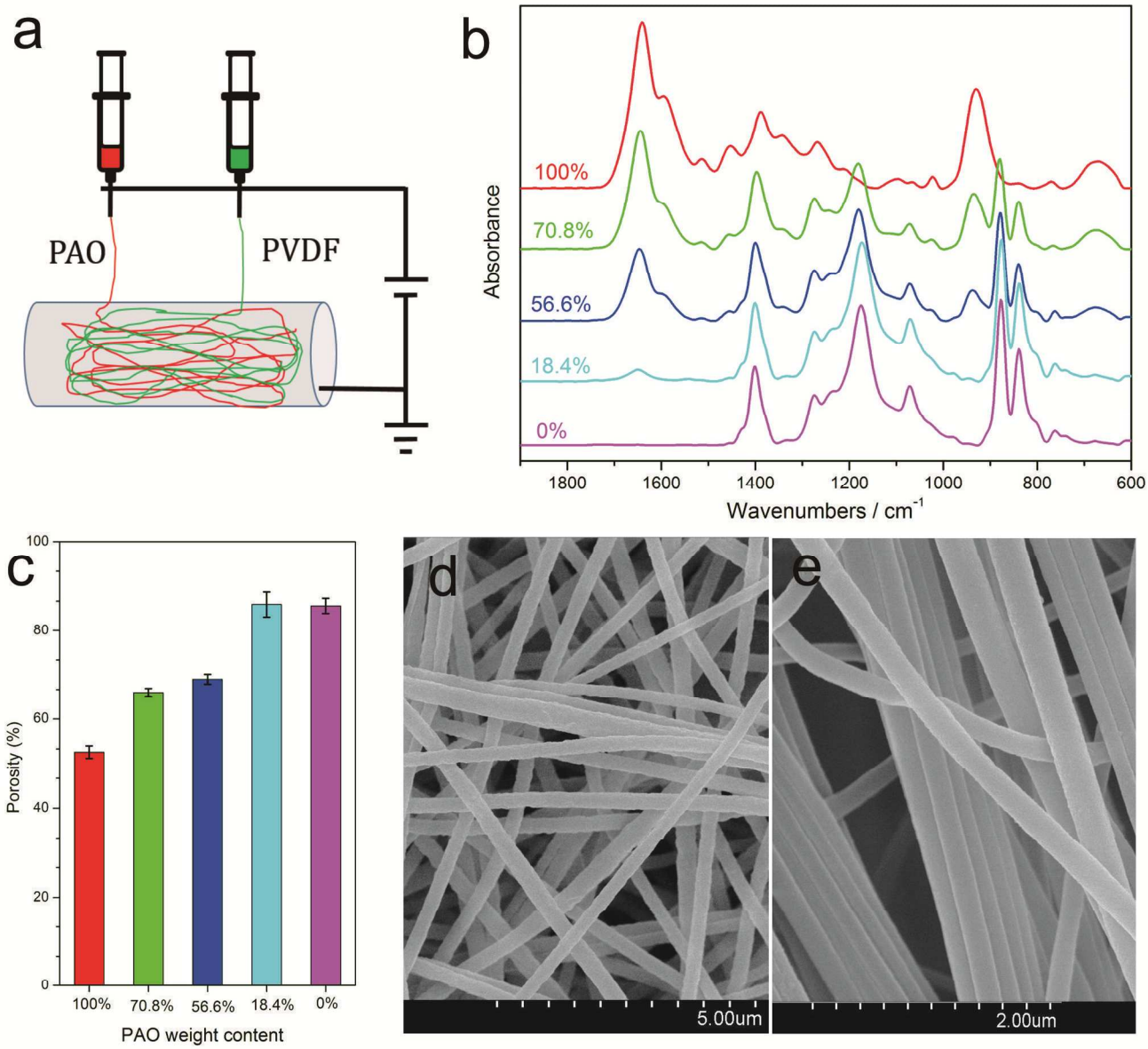

Fig.1 (a) Schematic diagram of two-nozzle electrospinning process for PAO/PVDF composite mats preparation; (b) FT-IR spectra and (c) porosity of electrospun nanofibrous mats with different content of PAO. SEM images of electrospun nanofibrous mats containing (d) 56.6% and (e) 100% of PAO.

Herein, we introduce a two-nozzle electrospinning process to avoid the poor miscibility of PAO.[29] As **Figure 1a** shows, PAO and polyvinylidene fluoride (PVDF) solutions are separately perfused in two syringes and connected to the high-voltage power source. PAO and PVDF nanofibers are simultaneously drawn out from their respective nozzles, and then interwoven into a uniform fibrous composite assembly, which is called a mat. Fibrous composite mats with different PAO contents can be achieved by controlling the injection rate of the PVDF solution (**Table S1**). The actual content of PAO in the mats was determined by microwave digestion, based on the different stabilities of the PVDF and PAO fibres (**Figure S1**). **Figure 1b** presents the FT-IR spectra of the electrospun fibrous mats with different PAO contents. The peaks at 1647 and 945 cm^{-1}, attributed to the characteristic peaks of the –C=N– and –N–O– bonds of the AO groups,[7] grow stronger as the PAO content in the composite mat increases.

As mentioned above, the electrospun fibrous mats are porous materials. Their porosity is an important parameter which influences the efficiency of adsorbent-seawater contact and

metal ion-uptake performance. BET nitrogen adsorption and Mercury porosimetry are the most popular methods adopted for the characterization of porosity of porous materials. Herein, we used BET nitrogen adsorption to estimate the surface area of PAO mats up to 41.6 $m^2 g^{-1}$, while the pore size range determined is just nanopores, which appears large deviation from SEM observation as shown in **Figure 1e** and **Figure S2a**. That may be reasoned as the irregular structure and outsize of pores formed by nanofibers interweaving. Therefore, just the nanopores in nanofibers have been determined. We further used Mercury porosimetry to determine pore size distribution of PAO mat, and found the pore size range detected is from 100 to 1000 nm, which is larger than that by BET nitrogen adsorption (**Figure S2b**). However, the higher pressures bore on mats would cause crushing and deformation of the pore network, which results in incorrect reporting of the pore volume and pore size distribution of very compliant materials, like electrospun nanofibrous mats.[30] Similar problems were also recorded in the study of xerogels and aerogels materials.[31]

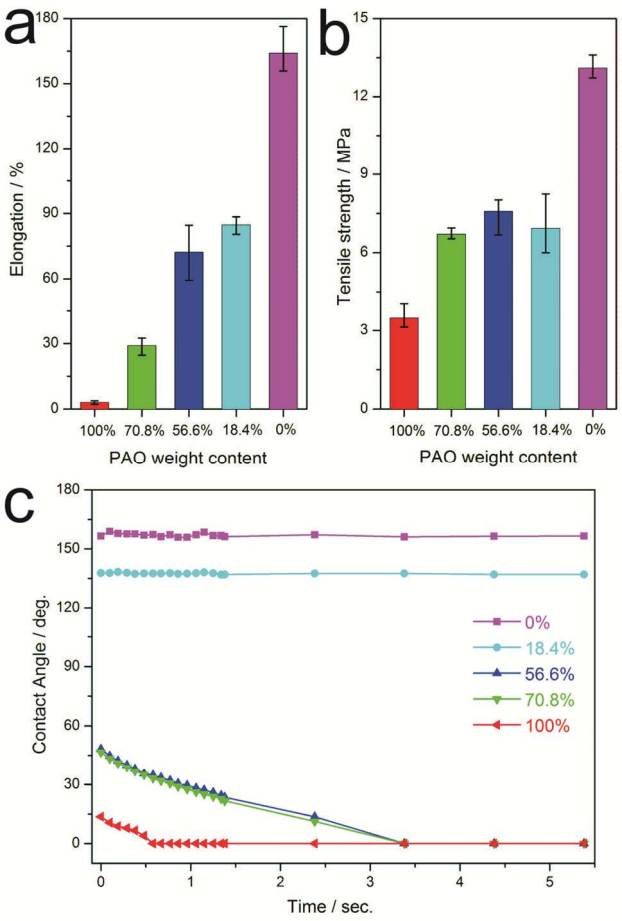

Fig.2 (a) Elongation, (b) Tensile strength and (c) Contact angle tests of electrospun nanofibrous mats with different content of PAO.

In this context, we conceived a simple method to determine porosity based on the inherent densities of PAO and PVDF, and the apparent density of the PAO/PVDF composite mats (details are provided in the ***ESI*, *Experimental Section S3*** and ***Table S2***).[25] As shown in **Figure 1c**, a PAO mat obtained by electrospinning exhibits about 56% porosity. When blended with PVDF during electrospinning, its porosity can be increased as the PVDF content increases. Notably, the porosity of the composite mat with 81.6% PVDF content is ~85% similar to that of the pure PVDF electrospun mat. The SEM images in **Figure 1d** and **Figure 1e** of the electrospun mats with 56.6% and 100% PAO content show that the diameters of the ultrafine fibres in the electrospun mats are all in the range from 150 to 400 nm. These nanofibers are overlapped crosswise and numerous pores pervade the whole mat (**Figure S3**).[25] Furthermore, in the PAO electrospun mat, many fibres were bundled together, perhaps by electrostatic attraction between them. However, this phenomenon was not observed in the nanofibrous PAO/PVDF composite mats (**Figure 1d**), which indicates that PVDF nanofibers are able to inhibit the adherence of PAO nanofibers during the two-nozzle electrospinning process. It may be reasoned that the strong polarity of the PVDF material disrupts the electrostatic force between the PAO nanofibers, makes them dispersing more uniformly.[32] For this reason, the porosity of nanofibrous PAO/PVDF composite mats is increased.

PVDF is a highly non-reactive, specialty plastic material that exhibits flexibility, high chemical corrosion resistance, heat resistance, and good weatherability. Its properties make it desirable as a skeletal polymer by which to enhance the PAO-based material by improving its poor mechanical properties. As **Figure 2a** and **Figure 2b** show, the tensile strength and elongation of pure PVDF nanofibrous mat are 13.1 MPa and 164.1%, respectively, matching with that reported previously.[33] It is observed that the mechanical properties of the PAO mats are very weak. When it was co-electrospun with PVDF into a single mat with different content, the tensile strength and elongation of resultant composite mats are obviously enhanced. The tensile strength and elongation are increased by at least two- and thirty-fold, respectively, which demonstrates the greater strength and flexibility of the nanofibrous PAO/PVDF composite mats. PVDF is a rather hydrophobic material, and the hydrophilicity of the nanofibrous PAO/PVDF composite mats should decrease with the PVDF content increasing; this is confirmed in **Figure 2c**. Fortunately, the hydrophilicity of the nanofibrous composite mats remains satisfactory when the PVDF content is less than 50%, so that water droplets can thoroughly infiltrate the membrane in only a few seconds. Considering that hydrophilicity is another important factor that influences the adsorption performance of the absorbents, and directly relates to the quantity of ions in the water that contact the functional groups, we must control the PVDF content below 50% to obtain hydrophilic, flexible, and reinforced nanofibrous PAO/PVDF mats.

To quickly evaluate the adsorption performance of the adsorbents in seawater, we designed a novel adsorption test method as described in the ***Experimental Section***. We prepared a simulated seawater solution at pH 8.0 with 3.5 wt.% sea salt and ten commonly found marine elements, including U, V, Fe, Co, Ni, Cu, Zn, Pb, Mg, and Ca, added at ~100 times their actual concentrations in real seawater.[34] All the ion concentrations are listed in **Table S3** and the preparation procedure of simulated seawater is provided in ***ESI*** as ***Experimental Section S4***. The electrospun mats with different PAO contents were immersed in 5 L of the simulated seawater for 24 hours with shaking at room temperature. There are two advantages of this design. First, this solution closely approximates actual seawater, which contains many ionic interferents. The assessment of adsorbents for uranium extraction would be more authentic than that from a pure uranyl solution. Second, increasing the concentration of the

uranium and other co-existing ions would be helpful in evaluating the long-term adsorption capacity of adsorbents in actual seawater (3.3 ppb). Based on the results of our other unpublished works, the adsorption capacity of adsorbents evaluated by this method represents that of about 25 days' simulated adsorption in actual seawater (3.3 ppb).

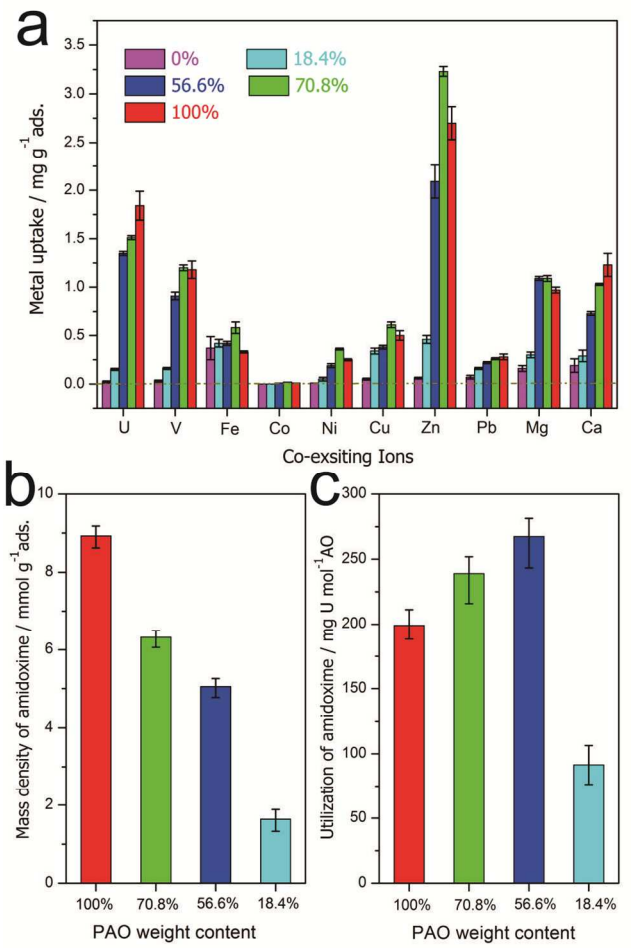

Fig.3 (a) Metal ions uptake capacity and (b) mass density amidoxime groups of electrospun nanofibrous mats with different PAO content; and (c) utilization of amidoxime groups to uranium uptake of electrospun nanofibrous mats with different PAO content.

After adsorption in the simulated seawater**,** the colour of electrospun nanofibrous mats here changes from white to yellow as **Figure S4** shows. This is an indication that some metal ions have been adsorbed. **Figure 3a** also shows that other interferents have been adsorbed on the nanofibrous mats; the Zn capacity is even higher than that of the uranyl ion. The existence of interferents will undoubtedly reduce the adsorption capacity of the uranyl ions. That is why some adsorbents have good adsorption capacity in pure uranyl solution, but unsatisfactory in real seawater. Meanwhile, the adsorption capacities for Mg and Ca are lower than that of uranium. Given their hundred-fold higher concentrations relative to the uranyl ion in seawater, we can conclude that that the AO-based adsorbents possess good selectivity for the uranyl ion compared to the massive amounts of Mg and Ca ions. It also shows that the adsorption capacity of the nanofibrous mats is slightly decreased from 1.86 to 1.35 mg U g^{-1} adsorbents as the PAO content decreases, until the PAO is decreased to 18.4%. **Figure 3b** shows that the mass density of the AO groups in these nanofibrous mats decreases as the PAO content decreases. **Figure 3c** illustrates an interesting trend in which the utilization of the AO functional groups in the electrospun mats increases as the PAO content decreases until 18.4%. In **Figure 1c**, we demonstrated that the porosity of the electrospun mats increases as the PAO content decreases. This indicates that the higher porosity improves the utilization efficiency of the AO groups in the nanofibrous mats, and makes a compensation for the decrease of PAO content, which reduces the capacity decrease of different nanofibrous mats, although there is substantial difference of PAO content. Admittedly, the uranium adsorption capacity of these mats is not better than that of conventional adsorbents from graft polymerization.[12, 20] However, relative to the 300%, even 600% degree of grafting PAO, the capacity of mats with such lower PAO content is acceptable in contrast. At this level, we can conclude that pursuit of high AO group content may not always be a prior option to improve the adsorption capacity of AO-based adsorbents. Therefore, efforts to enlarge the distribution of AO groups in such materials would be a feasible and novel strategy to prepare highly efficient adsorbents for uranium extraction. As for the decreased adsorption capacity and utilization of the nanofibrous composite mat at an 18.4% content of PAO, the lower hydrophilicity may be accountable (**Figure 2c**).

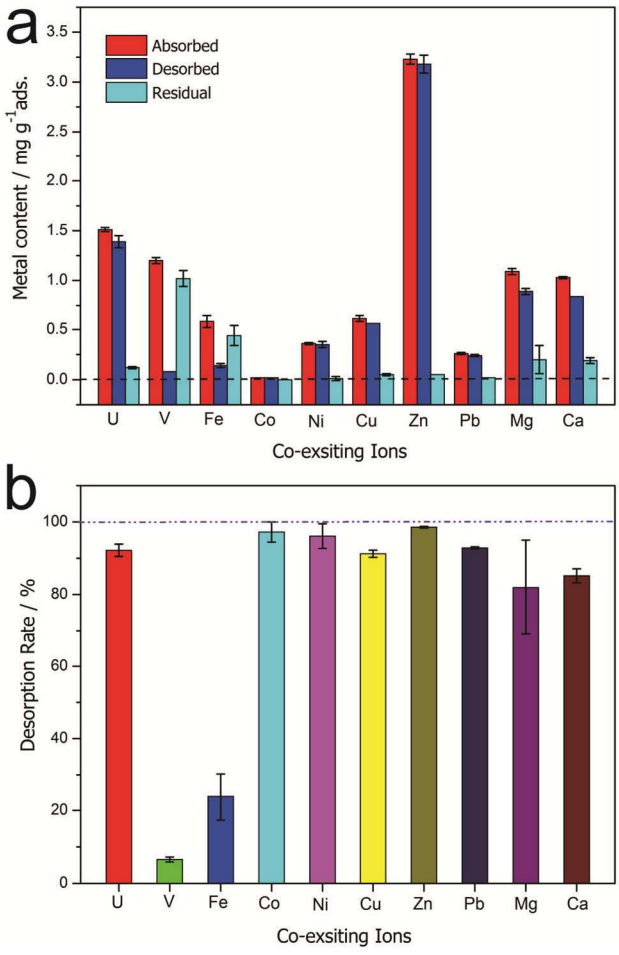

Fig.4 (a) The metal ions content adsorbed, desorbed and residual in electrospun nanofibrous mat with 70.8% of PAO; (b)

desorption rate of various metal ions of electrospun nanofibrous mat with 70.8% of PAO.

To rapidly investigate the desorption performance of the nanofibrous PAO/PVDF composite mats, an HCl solution (0.5 mol L^{-1}) was used as an eluent to desorb metal ions. After elution, the contents of the metal ions in the eluent solution (***desorbed***) and eluted mats (***residual***) were determined. The metal ion contents in the adsorbed nanofibrous composite mats (***adsorbed***) were also determined for comparison. In **Figure 4a**, it is clear that the uranyl and most of the other ions were desorbed after HCl solution treatment, except V and Fe. We calculated the desorption rate of all the absorbed metal ions in the nanofibrous composite mats; this data is presented in **Figure 4b**. It shows that about 92.2% uranium is eluted, whereas most of the vanadium (*ca*. 93.4%) remains on the desorbed nanofibrous composite mats. Thus, uranium and vanadium have different desorption behaviours during HCl elution, which is of consistency to previous work.[35] Furthermore, we investigated the recyclability of the nanofibrous PAO/PVDF composite mats by repeatedly adsorption and HCl elution (Figure S4a and S4b). It was found that HCl elution trends to damage the structure of mats. After third desorption, the mat was destroyed into little chips, which has been also confirmed by N. Seko *et al*.[10] The adsorption capacity of the third adsorption didn't decrease obviously (**Figure S4a**), although the desorption level of the second cycle decreased distinctly (**Figure S4b**). While the average adsorption capacity of these three adsorption cycles shows a 1.31 mg U g^{-1} adsorbent, which indicates the adsorption capacity of mat is reduced by HCl elution. Interestingly, the vanadium content is higher than first adsorption, which shows an accumulation effect in every cycle (**Figure S4a**). It is known that vanadium desorption requires very stronger acid solution (~5 mol L^{-1}) owing to its strong interaction with AO.[35] It can't be recovered in every adsorption/elution cycle, because strong acid treatment will destroy the adsorbent. However, the accumulation effect in every cycle would help us to obtained appreciable vanadium at the last cycle. Considering the good economic benefits of vanadium, it could bring the total running cost down of uranium extraction from seawater.

Conclusions

In summary, a novel design of nanofibrous AO-based adsorbents for uranium extraction was executed through a two-nozzle electrospinning process, using amidoxized PAN as a starting material. The electrospun PAO mat was confirmed to be highly porous, and after blending with PVDF nanofibers, the porosity and mechanical properties of the resultant nanofibrous PAO/PVDF composite mats were obviously enhanced, but still retained their high hydrophilicity. The adsorption tests in simulated seawater showed that the adsorption selectivity of the nanofibrous PAO/PVDF composite mats for the uranyl ion was still satisfactory, even in the presence of large amounts of interferents. Moreover, the availability of AO groups to adsorb uranyl ions was improved by the blending with the PVDF nanofibers in comparison to the pure PAO nanofibrous mat. Desorption tests suggested the good desorption selectivity of nanofibrous PAO/PVDF composite mats between uranyl and vanadium ions. Therefore, the two elements can be separated in desorption process. Overall, this novel approach through a two-nozzle electrospinning process effectively increases the adsorbent porosity and improves the utilization of the functional groups, which is significant in the development of highly effective adsorbents for uranium extraction from seawater. Inspired by this work, other materials with different functional organic compounds or nanoparticles can be prepared by this route to enhance their relative performance.

Experimental Section

Preparation of nanofibrous PAO/PVDF composite mats: The preparation of PAO was described in ***Experimental Section S2*** and ***Figure S6***of ***ESI***, and the chemical structure of PAO has been characterized by elemental analysis, FT-IR and XPS, which shown in **Table S3** and **Figure S7**. Herein, the electrospinning setup involved is a commercial equipment purchased from Shenzhen TONGLI micro & nano LTD. China (**Figure S8**). PVDF solution (0.1 g mL^{-1} in DMF) and the foregoing PAO solution were loaded into two syringes and assembled in respective microinjection pumps. Then, the two nozzles were connected to a high-voltage direct current power source, and fixed on a holder that moved from left to right repeatedly while aimed at a rotary drum. The PAO and PVDF nanofibers were electrospun simultaneously and interwoven uniformly into the nanofibrous composite mat. The obtained mat was immersed in deionized water for 48 hour to remove inorganic salts which were introduced during amidoximation. Then, the mat was dried at 60 °C for 24 hour in a vacuum oven. The parameters of the electrospinning process were set as follows: voltage, 15 kV; rotary drum speed, 500 rpm; holder speed, 10 cm min^{-1}; and PAO solution injection rate, 0.4 mL h^{-1}. PVDF exhibits high chemical corrosion resistance, so it can withstand microwave digestion. Given that PAO is easily decomposed in a microwave digestion system, the PAO content of the nanofibrous composite mats was determined by measuring the weight loss from the mats after microwave digestion and calculating the content using ***Equation 1***.

$$x(\%) = \frac{W_m - W_r}{W_m} \times 100\% \quad (1)$$

Where x is the weight content of the PAO in the nanofibrous composite mat; And W_m and W_r are the weights of the nanofibrous PAO/PVDF composite mat before and after microwave digestion. Therefore, nanofibrous composite mats with different content of PAO can be prepared by adjusting the injection rate of PVDF solution (as shown in **Table S1**).

Adsorption tests in simulated seawater: Nanofibrous mat samples (ca. 100 mg) were immerged in 5 L sea salt solution (3.5 wt.%, pH = 8.0) containing U, V, Fe, Co, Ni, Cu, Zn, Pb, Mg, and Ca ions; the concentration of each ion was 100 times that in real sea water (details in ***Experimental Section S4*** and **Table S3 of *ESI***). After shaking (100 rpm) for 24 hours at room temperature, the nanofibrous mats were retrieved, washed with copious water, and dried thoroughly in a vacuum oven. Then, the dried samples were digested with concentrated nitric acid in a MARS 6™ Microwave Digestion System from CEM Corporation, USA. The ion concentrations in the digestion solution were determined using a Perkin-Elmer Optima 8000 inductively coupled plasma–atomic emission spectrometer (ICP-AES). The U adsorption capacity of the nanofibrous mats was evaluated according to the concentration in the digestion solution. The formula for the calculation was as follows:

$$Q = \frac{M_U}{M_m} \quad (2)$$

Where Q is the adsorption capacity of nanofibrous mat; M_U is the weight of U in the digested solution from the adsorbed nanofibrous mats; and M_m is the weight of pristine nanofibrous mats used for the adsorption experiment.

Desorption Tests: The adsorbed mats were immersed in 0.5 mol L^{-1} HCl solution for a 30 minutes desorption period, retrieved, washed with water, dried in a vacuum oven, and decomposed by microwave digestion. The ion concentrations in desorption and digestion solutions were determined by ICP-AES. The desorption rate from the nanofibrous mats was calculated using ***Equation 3***.

$$d(\%) = \frac{M_{ds}}{M_{ds} + M_{dg}} \times 100\% \quad (3)$$

Where d is the desorption rate from the nanofibrous mat; and M_{ds} and M_{dg} are the weights of uranium in desorption and digestion solutions of the desorbed nanofibrous mats, respectively.

Acknowledgements

We greatly appreciate supports from the "Strategic Priority Research Program" of the Chinese Academy of Sciences (Grant XDA02040300), the "Knowledge Innovation Program" of the Chinese Academy of Sciences (Grant KJCX2-YW-N49)", and the National Natural Science Foundation of China (Grants 11305248, 11305241 and 11175234).

Notes and references

[a] *CAS Center for Excellence in TMSR Energy System, Shanghai Institute of Applied Physics, Chinese Academy of Sciences, No. 2019 Jialuo Rd., Jiading Dist., Shanghai, 201800, China. E-mail: zhangbowu@foxmail.com; jingyeli@sinap.ac.cn; Tel: +86-21-39194652; +86-21-39194505*

[b] *Graduate University of Chinese Academy of Sciences, No. 19A Yuquan Rd., Shijingshan Dist., Beijing, 100049, China*

‡ Miss S. Y. XIE and Miss X. Y. Liu contributed equally to this work.

† Electronic Supplementary Information (ESI) available: The experimental details of PAO preparation and measurement of porosity of nanofibrous mats. The Ions concentration and preparation procedure of simulated sea water. Elemental analysis, XPS and FT-IR spectrum of PAO, recyclability testing of nanofibrous mat. The SEM images of PAO/PVDF composite mats with different PAO content. The measurement of PAO content in composite mats. The pictures of different electrospun nanofibrous mats before and after adsorption. See DOI: 10.1039/b000000x/

1. IAEA and OECD/NEA, *Uranium 2014: Resources, Production and Demand*, International Atomic Energy Agency (IAEA) & Nuclear Energy Agency (NEA) of the Organisation for Economic Co-operation and Development (OECD), 2014.
2. R. V. Davies, J. Kennedy, R. W. McIlroy, R. Spence and K. M. Hill, *Nature*, 1964, **203**, 1110-1115.
3. M. Kanno, *J Nucl Sci Technol*, 1984, **21**, 1-9.
4. L. Rao, *Recent International R&D Activities in the Extraction of Uranium from Seawater*, Lawrence Berkeley National Laboratory, 2011.
5. C. W. Abney, S. Liu and W. Lin, *J. Phys. Chem. A*, 2013, **117**, 11558-11565; P. S. Barber, S. P. Kelley and R. D. Rogers, *RSC Adv.*, 2012, **2**, 8526-8530; S. Vukovic, L. A. Watson, S. O. Kang, R. Custelcean and B. P. Hay, *Inorg. Chem.*, 2012, **51**, 3855-3859.
6. M. M. Aly and M. F. Hamza, *J. Dispersion Sci. Tech.*, 2012, **34**, 182-213; S.-H. Choi, M.-S. Choi, Y.-T. Park, K.-P. Lee and H.-D. Kang, *Radiat. Phys. Chem.*, 2003, **67**, 387-390; K. Oshita, A. Sabarudin, T. Takayanagi, M. Oshima and S. Motomizu, *Talanta*, 2009, **79**, 1031-1035; H. Egawa, N. Kabay, T. Shuto and A. Jyo, *Ind. Eng. Chem. Res.*, 1993, **32**, 540-547.
7. S.-H. Choi and Y. C. Nho, *Radiat. Phys. Chem.*, 2000, **57**, 187-193.
8. A. Y. Zhang, T. Asakura and G. Uchiyama, *React Funct Polym*, 2003, **57**, 67-76.
9. N. Seko, A. Katakai, S. Hasegawa, M. Tamada, N. Kasai, H. Takeda, T. Sugo and K. Saito, *Nucl Technol*, 2003, **144**, 274-278; L. Rao, *J. Isotopes*, 2012, **25**, 129-139; K. Sekiguchi, K. Saito, S. Konishi, S. Furusaki, T. Sugo and H. Nobukawa, *Ind. Eng. Chem. Res.*, 1994, **33**, 662-666.
10. N. Seko, A. Katakai, M. Tamada, T. Sugo and F. Yoshii, *Sep. Sci. Tech.*, 2004, **39**, 3753-3767.
11. H. Chi, X. Liu, H. Ma, X. Yang, M. Yu, J. Zhang, M. Wang, J. Li and H. H. N. Seko, *Nucl. Sci. Tech.*, 2014, **25**, 010302; J. Kim, Y. Oyola, C. Tsouris, C. R. Hexel, R. T. Mayes, C. J. Janke and S. Dai, *Ind. Eng. Chem. Res.*, 2013, **52**, 9433-9440; H. Liu, M. Yu, H. Ma, Z. Wang, L. Li and J. Li, *Radiat. Phys. Chem.*, 2014, **94**, 129-132; H. Liu, M. Yu, B. Deng, L. Li, H. Jiang and J. Li, *Radiat. Phys. Chem.*, 2012, **81**, 93-96; X. Liu, H. Liu, H. Ma, C. Cao, M. Yu, Z. Wang, B. Deng, M. Wang and J. Li, *Ind. Eng. Chem. Res.*, 2012, **51**, 15089-15095.
12. T. Saito, S. Brown, S. Chatterjee, J. Kim, C. Tsouris, R. T. Mayes, L.-J. Kuo, G. Gill, Y. Oyola, C. J. Janke and S. Dai, *J. Mater. Chem. A*, 2014, **2**, 14674-14681; Z. Xing, J. Hu, M. Wang, W. Zhang, S. Li, Q. GAO and G. Wu, *Sci. China Chem.*, 2013, **56**, 1504-1509.
13. E. Schneider and D. Sachde, *Sci. Global Sec.*, 2013, **21**, 134-163; J. Kim, C. Tsouris, Y. Oyola, C. J. Janke, R. T. Mayes, S. Dai, G. Gill, L.-J. Kuo, J. Wood, K.-Y. Choe, E. Schneider and H. Lindner, *Ind. Eng. Chem. Res.*, 2014, **53**, 6076-6083; T. Sugo, M. Tamada, T. Seguchi, T. Shimizu, M. Uotani and R. Kashima, *J. Atom. Energ. Soc. Jpn*, 2001, **43**, 1010-1016.
14. Y. Wang, Z. Gu, J. Yang, J. Liao, Y. Yang, N. Liu and J. Tang, *Appl. Surf. Sci.*, 2014, **320**, 10-20.
15. A. Deb, P. Ilaiyaraja, D. Ponraju and B. Venkatraman, *J Radioanal Nucl Chem*, 2012, **291**, 877-883.
16. Y. Zhao, J. Li, S. Zhang, H. Chen and D. Shao, *RSC Adv.*, 2013, **3**, 18952-18959; D. Shao, J. Li and X. Wang, *Sci. China Chem.*, 2014, 1-10.
17. W. Yang, Z.-Q. Bai, W.-Q. Shi, L.-Y. Yuan, T. Tian, Z.-F. Chai, H. Wang and Z.-M. Sun, *Chem. Commun.*, 2013, **49**, 10415-10417; M. Carboni, C. W. Abney, S. Liu and W. Lin, *Chem. Sci.*, 2013, **4**, 2396-2402.
18. J. L. Vivero-Escoto, M. Carboni, C. W. Abney, K. E. deKrafft and W. Lin, *Microporous Mesoporous Mater.*, 2013, **180**, 22-31; P. J. Lebed, J.-D. Savoie, J. Florek, F. Bilodeau, D. Larivière and F. Kleitz, *Chem. Mater.*, 2012, **24**, 4166-4176; S. Kerisit and C. Liu, *Environ. Sci. Tech.*, 2014, **48**, 3899-3907.
19. Y. Zhao, J. Li, S. Zhang and X. Wang, *RSC Adv.*, 2014, **4**, 32710-32717; Y. Zhao, J. Li, L. Zhao, S. Zhang, Y. Huang, X. Wu and X. Wang, *Chem. Eng. J.*, 2014, **235**, 275-283.
20. Y. Yue, R. T. Mayes, J. Kim, P. F. Fulvio, X. G. Sun, C. Tsouris, J. Chen, S. Brown and S. Dai, *Angew.Chem. Int. Ed.*, 2013, **52**, 13458-13462.
21. Y. Yue, X. Sun, R. T. Mayes, J. Kim, P. F. Fulvio, Z. Qiao, S. Brown, C. Tsouris, Y. Oyola and S. Dai, *Sci. China Chem.*, 2013, **56**, 1510-1515; J. Gorka, R. T. Mayes, L. Baggetto, G. M. Veith and S. Dai, *J. Mater. Chem. A*, 2013, **1**, 3016-3026.
22. V. Thavasi, G. Singh and S. Ramakrishna, *Energy Environ. Sci.*, 2008, **1**, 205-221; D. Li and Y. Xia, *Adv. Mater.*, 2004, **16**, 1151-1170.

23. S. Cavaliere, S. Subianto, I. Savych, D. J. Jones and J. Roziere, *Energy Environ. Sci.*, 2011, **4**, 4761-4785.
24. H. Yuan, S. Zhao, H. Tu, B. Li, Q. Li, B. Feng, H. Peng and Y. Zhang, *J. Mater. Chem.*, 2012, **22**, 19634-19638.
25. X. Zhu, W. Cui, X. Li and Y. Jin, *Biomacromolecules*, 2008, **9**, 1795-1801.
26. L. D. Tijing, J.-S. Choi, S. Lee, S.-H. Kim and H. K. Shon, *J. Membr. Sci.*, 2014, **453**, 435-462.
27. S. Agarwal, A. Greiner and J. H. Wendorff, *Prog. Polym. Sci.*, 2013, **38**, 963-991; Z.-M. Huang, Y. Z. Zhang, M. Kotaki and S. Ramakrishna, *Compos. Sci. Tech.*, 2003, **63**, 2223-2253; C. J. Luo, S. D. Stoyanov, E. Stride, E. Pelan and M. Edirisinghe, *Chem. Soc. Rev.*, 2012, **41**, 4708-4735.
28. M. Chen, C. Wang, W. Fang, J. Wang, W. Zhang, G. Jin and G. Diao, *Langmuir*, 2013, **29**, 11858-11867; Y. Wang, W. Li, X. Jiao and D. Chen, *J. Mater. Chem. A*, 2013, **1**, 10720-10726; P. S. Barber, S. P. Kelley, C. S. Griggs, S. Wallace and R. D. Rogers, *Green Chem.*, 2014, **16**, 1828-1836.
29. C. Zhang, Y. Li, W. Wang, N. Zhan, N. Xiao, S. Wang, Y. Li and Q. Yang, *Eur. Polym. J.*, 2011, **47**, 2228-2233.
30. G. C. Rutledge, J. L. Lowery and C. L. Pai, *J. Eng. Fiber. Fabr.*, 2009, **4**, 1-13; J. L. Lowery, N. Datta and G. C. Rutledge, *Biomaterials*, 2010, **31**, 491-504.
31. R. Pirard, B. Heinrichs, O. Van Cantfort and J. P. Pirard, *J. Sol-Gel Sci. Technol.*, 1998, **13**, 335-339.
32. D. Christopher, W. Xianyan, A. S. Lynne and K. Jayant, in *Polymeric Nanofibers*, American Chemical Society, 2006, vol. 918, pp. 137-148.
33. R. Nakashima, K. Watanabe, Y. Lee, B.-S. Kim and I.-S. Kim, *Adv. Polym. Techn.*, 2013, **32**, E44-E52.
34. J. Kim, C. Tsouris, R. T. Mayes, Y. Oyola, T. Saito, C. J. Janke, S. Dai, E. Schneider and D. Sachde, *Sep. Sci. Tech.*, 2012, **48**, 367-387.
35. T. Suzuki, K. Saito, T. Sugo, H. Ogura and K. Oguma, *Anal. Sci.*, 2000, **16**, 429-432.

Graphic Abstract

A novel amidoxime (AO)-based adsorbent, integrating the high affinity of AO groups and size effect of nanomaterials in nanofibrous composite mats has been prepared by two-nozzle electrospinning process, for the uranium extraction from seawater.